Laboratory Pullout Test of Geogrid Reinforcements for Submerged Mechanically Stabilized Earth for Waterfront Applications

Allan E. Botuyan[1, 2*] and Glen A. Lorenzo[3]
[1]College of Engineering and Technology
Mindanao State University – Iligan Institute of Technology
Iligan City, 9200 Philippines

[2]Qualitest Solutions & Technologies Inc. (QSTI)
Davao City, 8000 Philippines
[*]*aebdavao@gmail.com*

[3]Civil Engineering Department
Mindanao State University – Marawi
Marawi City, 9700 Philippines

Date received: November 15, 2019
Revision accepted: October 5, 2020

Abstract

The design and evaluation of mechanically stabilized earth (MSE) wall structures for riverbank protection, quays, sea walls and other waterfront structures is critically dependent on a design parameter called the interaction coefficient (Ci) for submerged or fully saturated condition. However, the available research works conducted in this field are limited to non-submerged and, at most, partially saturated condition. This limitation does not closely represent actual conditions where waterfront structures are almost often submerged and fully saturated. Hence, the objective of this study was to determine the Ci in a submerged condition, on top of the Ci in a non-submerged condition for different types of geogrid reinforcement for fine-grained soils and coarse-grained soils used for MSE walls. Test results revealed that the Ci decreased as the effective overburden stress increased. The submerged conditions yielded lower Ci compared with non-submerged conditions, and the reduction was significant at a lower effective overburden stress for high density polyethylene uniaxial geogrid than the polyvinyl coated polyester yarn. The design parameters derived from these conditions can be used for the evaluation and design of MSE walls for waterfront applications with a higher level of confidence.

Keywords*:* mechanically stabilized earth, interaction coefficients, pullout test, geogrid reinforcement

1. Introduction

Existing mechanically stabilized earth (MSE) was designed for drainage conditions, by allowing, at most, a temporary saturation by incorporating

efficient drainage at the back and toe of the MSE in the attempts of eliminating the detrimental effects of saturation (Alfaro *et al*., 1995a). Therefore, the use of free-draining backfill such as sand or gravel is necessary. However, despite the free-draining backfill, the possibility of permanent saturation or constant submergence of MSE is highly likely. This could be due to the continuous flooding of rivers caused by heavy rains aggravated by increased siltation at deltas and/or constriction of river widths at densely populated areas.

Many laboratory pullout tests of the reinforced soils in the past 30 years were conducted in the drained condition where the soil specimen is either dry (Peterson and Anderson, 1980; Jewell *et al*., 1984; Bergado *et al*., 1988, 1986, 1992, 1993, 1996; Palmeira and Milligan, 1989; Rimoldi *et al*., 1994; Alfaro *et al*., 1995b; Mitchell and Zornberg, 1995; Matsui *et al*., 1996; Ochiai *et al*., 1996; Lopes and Lopes, 1999; Muller-Rochholz and Recker, 2000; Montanelli and Recalcati, 2003; Duszynska and Bolt, 2004; Farrag and Morvant, 2004; Bathurst *et al*., 2005; Moraci and Gioffre, 2006; Moraci and Recalcati, 2006; Hossain and Sakai, 2007; Palmeira, 2007; Moraci and Cardile, 2009, 2012; Berg *et al*., 2009; Nayeri and Fakharian, 2009; Sieira *et al*., 2009; Esfandiari and Selamat, 2012; Zhou *et al*., 2012; Lajevardi *et al*., 2013; Minažek and Mulabdić, 2013; Moraci *et al*., 2014), or moist to some degree (Alfaro *et al*., 1995a). The results of the various studies were specifically applied to retaining structures on "dry ground" such as highway embankments and slope stabilization projects. A closely related study to the present work is on the design of MSE walls for fully saturated conditions by Bobet (2002). The study was conducted on steel-grid-reinforced-sands mixed with different percentages of silt. The comparison of the behaviors of the same condition was made for both drained and undrained setup. In general, there is little study conducted on submerged pullout test.

In contrast, the laboratory tests in this study were conducted on extensible high-density polyethylene (HDPE) uniaxial geogrids and polymer coated polyester uniaxial geogrids yarns for both drained and undrained conditions using fine-grained and coarse-grained backfill soils. Also, the procedure in the design and evaluation of saturated or submerged MSE walls in research studies of Bowles (1997), Jewell (1996), Koerner (2005), and the U.S. Department of Transportation and Federal Highway Administration (2001) adopted the effective stress principle. They also used the same unsaturated design parameters for submerged and non-submerged conditions such as the interaction coefficient (Ci). In this study, the design parameters were established by simulating large-scale pullout test for actual submerged and non-submerged conditions, separately.

2. Methodology

The study was carried out by fabricating a fully automated large-scale pullout box capable of carrying out the series of soil-geogrid simulation tests (American Society for Testing and Materials [ASTM] D6706-01, 2001) for both non-submerged and submerged conditions, complete with real-time electronic data acquisition system based on other works (ASTM D3080-04, 2004). The plan and section of the pullout box with submerged capability, schematic diagram, and photograph are shown in Figures 1, 2 and 3, respectively.

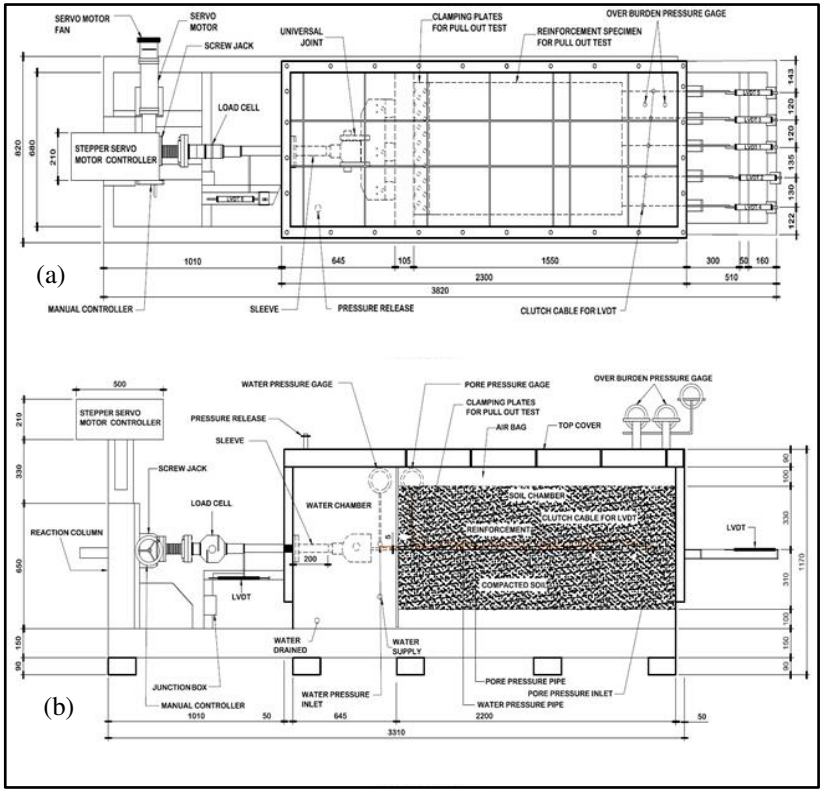

Figure 1. Plan (a) and section (b) of large-scale pullout box

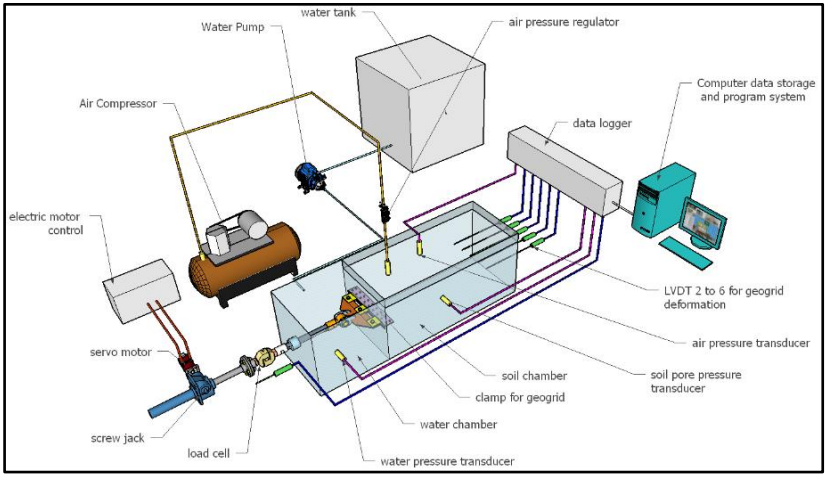

Figure 2. Schematic diagram of large pullout box with submerged capability

Figure 3. Fully automated large-scale pullout box with submerged capability

The simulation test was conducted by incorporating the effects of full saturation of the soil for different equivalent depths of submergence. The results of the pullout test were compared with test results on soils that were not submerged to compare the behaviors between the different drainage conditions.

The strength envelopes, defined by friction angle (F) and cohesion (c) of each of the type of soils, were determined using the large-scale direct shear box as a complementary test (ASTM D3080-04, 2004). The plan and section of the direct shear box and actual shear box are shown in Figures 4 and 5, respectively. Routine mechanical and physical laboratory tests were conducted on the two kinds of soils used to determine the properties such as the unit weight, Atterberg's limits, optimum moisture content, maximum dry density and soil classification, among others.

Two types of geogrids were used in this study: high density polyethylene (HDPE) Tensar RE580 uniaxial geogrids and the Polymer-coated Polyester Yarns (PPY) Tencate Miragrid GX60/30 uniaxial geogrids for two types of soils. These were coarse grained soils (CGS) and fine-grained soils (FGS) at different overburden pressures and at different simulated depths of submergence.

2.1 Test Setup, Sample Preparations and Measurements

Generally, the test procedures were divided into three major parts. First, preliminary laboratory test procedures were conducted to determine the physical and mechanical properties of the soil used for the pullout tests. Second, large-scale direct shear tests were employed to determine the strength parameters of the soil samples, such as the friction angle and cohesion values. Lastly, large-scale pullout tests were carried out on the geogrid reinforced soil for drained and undrained conditions for different types of geogrids and soils, and normal and pore pressures.

2.1.1 Preliminary Laboratory Test

From the mentioned soil samples, preliminary laboratory tests were conducted to establish the data needed prior to the direct shear tests and pullout tests. As mentioned, there were only two types of soil tested: FGS and CGS. The following were the laboratory tests that were undertaken for the soil samples:

Grain size analysis (ASTM D422-63, 1998) determined the particle size distribution of the soil to aid its classification. The content of sand, clay and silt were also determined.

Standard test for liquid limit, plastic limit and plasticity index of soils (ASTM D4318-10, 2010) was used to identify the moisture content at the boundary of

a liquid to semi-solid state of the soil (liquid limit) and the moisture content at the boundary of a solid to semi-solid state of the soil (plastic limit).

Standard proctor test (ASTM D698-12, 2012) was utilized to examine the moisture-density relationship, specifically the maximum dry density (MDD) and the optimum moisture content (OMC). The data was used during the soil compaction inside the pullout box.

Field density test (ASTM D1556-00, 2000) was applied to ascertain the in-situ density of the soil installed inside the pullout box. The compacted soil must be at least 95% of the MDD. This test procedure was conducted when the soil chamber was filled and compacted ready for dry and submerged conditions.

Specific gravity test (ASTM C127-01, 2001; ASTM C128-01, 2001) determined the weight and density properties of the soil by calculating the index properties of the soil samples.

Unified soil classification system (ASTM D2487-11, 2011) test classified the type of soil, generally as coarse-grained or fine-grained. They were further classified into more specific groupings (SC, SM, ML, and CL).

2.1.2 Large-Scale Direct Shear Test Equipment

The large-scale direct shear box (680 mm x 1200 in area and 400 mm deep) was developed and fabricated by the authors with a digitally programmed instrumentation from National Instruments for real-time measurement of pressures, forces, and displacements using automatic digital data loggers. Figure 4 shows the plan and section of the large-scale direct shear box. Figure 5 shows a photograph of the large-scale shear box with analog pressure gauge coupled with pressure transducer to measure the air bag pressure to simulate the overburden normal pressure. This equipment was fabricated for the purpose of determining the shear strength parameters of the soils used in the research, specifically the CGS and FGS.

2.1.3 Large-Scale Shear Box Test Procedure

The soil was compacted to a minimum of 95% of the MDD of the soil at every 200 mm layer using the OMC of the soil. After which, the airbag was placed on top of the soil. The lid was positioned and bolted on top of the airbag while securing the air pressure line and gauges on top.

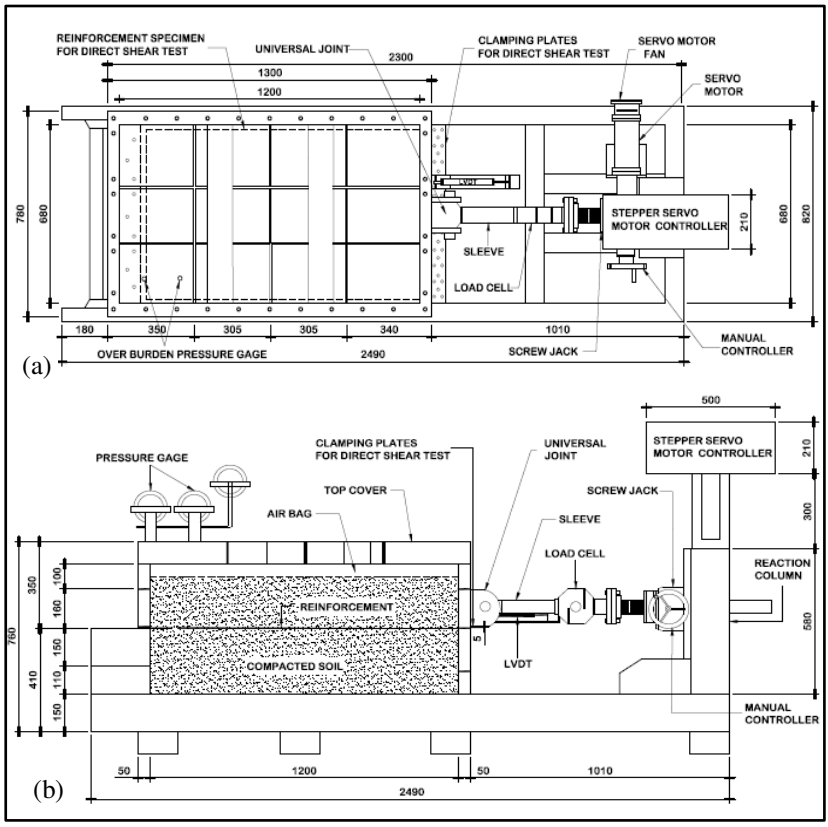

Figure 4. Plan (a) and section (b) of large-scale direct shear box

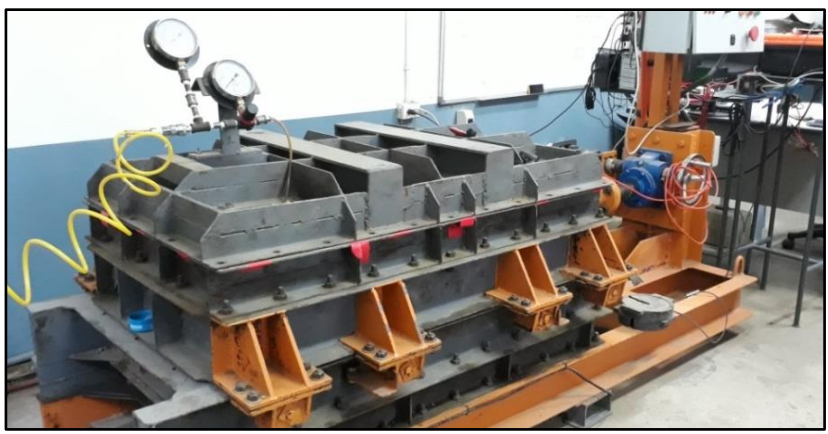

Figure 5. Large-scale direct shear box

Thereafter, a normal pressure on top of the compacted soil was placed using an airbag with a constant air pressure from a regulated electric pump. The shearing force was then applied to the top portion of the box at a rate of 1 mm/min. The load continued until failure which was manifested by a drop of load resistance. The system is fully automatic direct shear box with graphical user interface (GUI) and real-time data acquisition system (DACS) with pulse width modulator to record the force-displacement graph of the test.

2.1.4 Large-Scale Pullout Test Equipment

The authors also designed and fabricated the large pullout testing machine with submerged capabilities for this research as shown in Figure 1. The schematic diagram is shown in Figure 2 and a photograph is shown in Figure 3. The large pullout box was made of two chambers: (1) the soil-geogrid chamber with an inside dimension of 1500 mm length x 700 mm width x 740 mm height and (2) the water chamber with inside dimension of 600 mm length x 700 mm width x 740 mm height. A schematic diagram of the pullout box assembly as shown in Figure 2 consisted five elements which are as follows:

Mechanical Pullout Force Loading Device

The assembly provided an adjustable constant rate of displacement from, say, 1 mm/min to 10 mm/min, or as required by the test. The system was primarily pulled/pushed by a stepper motor (ES-MH234120, Leadshine, China) a 2 phase NEMA 42 size with 12.0 N-m holding torque. It was connected to a 1:30 gearbox speed reducer to further reduce the speed and increase torque. It was further connected to a 15-ton worm gear screw jack (JACTON, China) with a ratio of 1/32 or 0.3125 mm linear movement per full rotation of the shaft. The servo motor with electric motor control regulated the speed, direction and range of movement.

Rectangular Steel Box

There were two parts of the rectangular steel box: the soil chamber and the water chamber. The soil chamber had internal dimensions of 1.50 x 0.68 x 0.68 m (length x width x height) with steel sleeves of 0.20 m long reducing the effects of the front wall, where the clamping of the geogrid was located. This soil chamber where the reinforced soil is installed is shown in Figure 2. The water chamber had dimensions of 700 mm x 680 mm x 620 mm. It was located adjacent to and in front of the soil chamber. A pressure pump

controlled and fixed the simulated pore pressure in the water chamber that was attached adjacent to the soil chamber. The water chamber was connected to the soil chamber through the small perforation at the base of the soil chamber that was covered by highly permeable filters as shown in Figure 2.

Water Pressure System

The water pressure system simulated the height of submergence of the soil in the chamber. This was for the undrained loading condition where the soil chamber was fully saturated. The pressure is generated by a 0.8 kW centrifugal water pump (Eurostar, Italy) with a discharge capacity of 50 L/min and pressure head 10 m with plumbing line supplying the water chamber of the rectangular box. To regulate the required pressure, a gate valve was installed in the line to allow a certain amount of water to go out back to the reservoir while maintaining the desire pressure. The pressures were read from both chambers in the box making sure that they were of equal pressures.

Measuring Device

The pullout force was measured by a load cell outside the water chamber, as shown in Figure 19. It is an S-type 15-ton capacity tension-compression capable load cell (ZheJiang Tugong Instrument Co., Ltd., China).

The displacements in the geogrid specimen from the front wall and at some points along the length of the geogrid (e.g. at the transverse ribs of the geogrids) was measured using the electronic Linear Variable Displacement Transducers (LVDT) attached at the end portion of the soil chamber. The LVDT was a 150 mm stroke direct current 4 to 20 mA (Zhejiang Tugong Instruments Co., Ltd., China). There were five LVDTs installed at different locations in the geogrid connected to the transverse ribs and one LVDT at the load cell. The load and the six LVDTs were all connected to the Data Acquisition System.

Data Acquisition System (DAS)

It was used for continuous recording on the force applied on the geogrid, displacements of the chosen measuring points along the geogrid specimen, pressures on the water and soil chambers, and the pressure on the equivalent overburden pressure. A simultaneous recording of two-second reading interval of all the measuring instruments was collected by the DACS for the

entire duration of the test until the criteria for failure was achieved. The data collection was from the following sensors: six LVDTs from geogrid displacement, one load cell for applied pullout force, one pressure transducer for pore pressure reading in the soil chamber, one pressure transducer for pressure reading in water chamber, one pressure transducer for air pressure readings in the airbag, and one thermal transducer for water temperature in the water chamber.

The DAS employed the voltage input modules from National Instruments for accurate readings, specifically using the NI 9201 analog eight channel input module (National Instruments, USA) for CompaqDAQ (National Instruments, USA) and the NI 9237 four channel simultaneous bridge module CompaqDAQ (National Instruments, USA). Figure 21 shows the assembly of the DACS with the controls and computer storage of data.

2.2 Pullout Test Procedure

The pullout test was generally divided into two categories – (1) drained and (2) undrained loading conditions. Generally, the drained condition refers to the soil that can be unsaturated, and partially and fully saturated but water was free to drain when loaded. In other words, there was zero pore pressure in the soil when the pullout test was conducted. On the other hand, the undrained condition refers to the soil that is fully saturated and that there was pore-pressure between the soil particles during the loading and simulating the height of the submergence of the soil-geogrid interface.

Within each of these loading conditions, there were two types of soils used to interact with two types of geogrids: one was CGS and the other one was the FGS. Each geogrid type was tested for three different normal pressures simulating different overburden heights. For the drained loading conditions, the test did not include pore pressures while for the undrained condition, an additional constant pore pressure was added to the system to simulate three different water table depths.

In Table 1, tests numbered one to 12 were all in the drained loading condition, hence, the zero pore pressure values, and tests numbered 13 to 24 were in the undrained loading condition. Furthermore, the pull load rates for the drained and undrained loading conditions were 1 mm/min and 10 mm/min, respectively.

For the drained conditions, the total overburden pressure was equivalent to the effective overburden pressure. On the other hand, for the undrained condition, the effective overburden pressure was the total overburden pressure subtracted by the applied pore pressure. The pullout behavior from drained conditions and undrained conditions were then compared, evaluated, and made as the basis for establishing the design parameters for submerged MSE walls.

Table 1. Summary of large-scale pullout test

Test No.	Set No.	Soil Type	Geogrid Name	Loading Condition	Normal Pressure (kPa)	Pore Pressure (kPa)
1	1	CGS	Tensar RE580	Drained	20	0
2					41	0
3					62	0
4	2	CGS	Miragrid GX60/30	Drained	20	0
5					41	0
6					62	0
7	3	FGS	Tensar RE580	Drained	20	0
8					41	0
9					62	0
10	4	FGS	Miragrid GX60/30	Drained	20	0
11					41	0
12					62	0
13	5	CGS	Tensar RE580	Undrained	20	14
14					41	24
15					62	34
16	6	CGS	Miragrid GX60/30	Undrained	20	14
17					41	24
18					62	34
19	7	FGS	Tensar RE580	Undrained	20	14
20					28	24
21					34	34
22	8	FGS	Miragrid GX60/30	Undrained	20	10
23					28	13
24					34	17

2.2.1 Drained Loading Condition

Initially, the soil was placed and compacted at 150 mm lifts inside the soil chamber up to the level of the steel sleeve, which was the location of the geogrid. The field density test, designated as ASTM D1556-00 (2000) or its equivalent electric density gauge test, was conducted for each layer. The thickness of this soil under the geogrid was 300 mm. The desired degree of compaction was at least 95% of the maximum dry density and tested using the electronic soil density gauge.

The geogrid was then laid on this level and one end was connected to the grip plate that was connected to the tension rod inside the water chamber. The preparation of the geogrid specimen is as follows:

Tensar RE580

The size of the specimen was 1207 mm long x 600 mm wide. There were 27 longitudinal legs and six transverse ribs. Since the clamping zone was covered with steel plate with a width of 135 mm, the shear zone, which was the soil-geogrid interaction area reduced to 1072 mm x 600 mm. Figure 6 shows the prepared sample for the pullout test.

Figure 6. Tensar RE580 sample for the pullout tests

Tencate Miragrid GX60/30

The size of the specimen was 735 mm long x 590 mm wide. There were 24 longitudinal legs and 29 transverse supports. Since the clamping zone was covered with steel plate with a width of 135 mm, the shear zone, which was the soil-geogrid interaction area, was reduced to 585mm x 590mm. The shorter length of this sample than the Tensar RE580 was chosen since the Tencate Miragrid GX60/30 would fail by tension rather than pullout at higher confining pressures. Figure 7 shows the prepared sample for the pullout test.

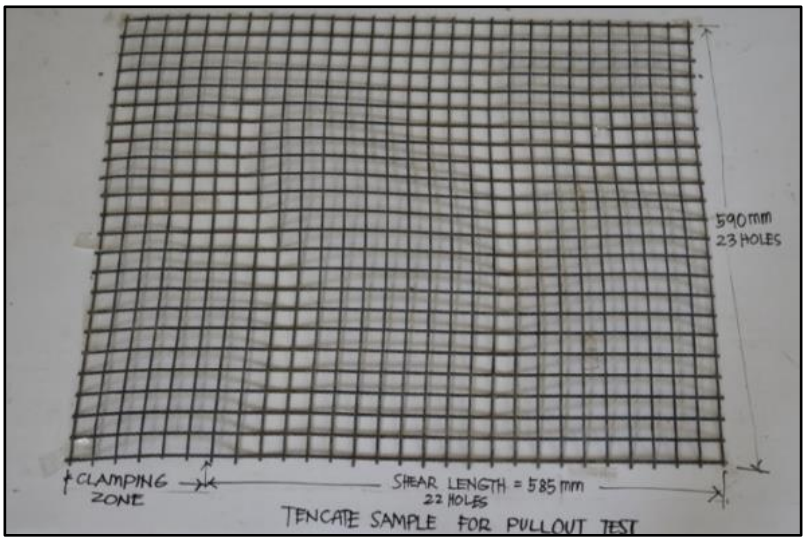

Figure 7. Tencate Miragrid GX60/30 sample for the pullout tests

The laboratory pullout test results were load-displacement curves for different confining pressures at a constant rate for each of the geogrid specimen tested. For each test, there was an average of six load-displacement curves. The first curve was for the unburied portion of the geogrid while the other five curves were for the different measured locations along the length of the geogrid tested. For the Tensar RE580, the locations measured were spaced at every transverse rib that was 250 mm. Figure 8 shows the locations in the measured geogrid. For Tencate Miragrid GX 60/30, the points of interest were spaced at every 100 mm as shown in Figure 9.

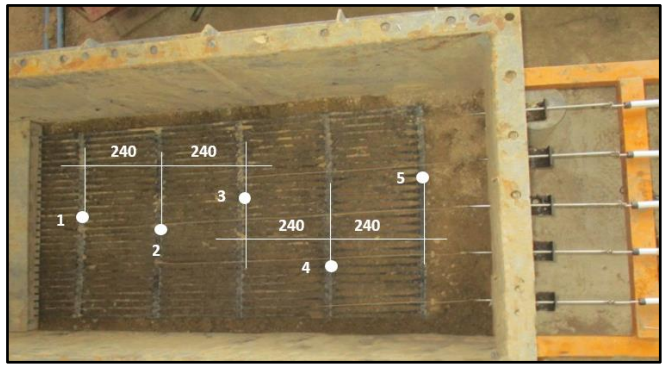

Figure 8. Typical location of displacement measurements for Tensar RE580

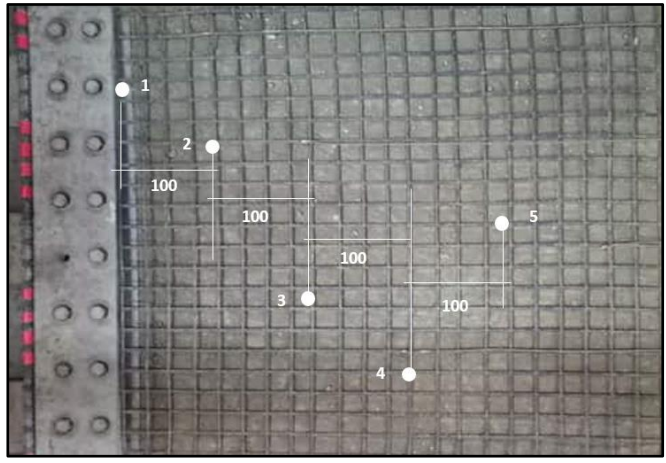

Figure 9. Typical location of displacement measurements for Tencate Miragrid GX60/30

The locations of the points of measurements were installed at the transverse ribs and distributed along the entire length of the geogrid tested. The ends of the rods were then connected to the respective LVDTs installed outside the pullout box. As shown in Figure 8, for the Tensar RE580, the typical locations of the point of measurements are shown in Table 2.

Table 2. Typical locations of the point of measurements for Tensar RE580

LVDT No.	From clamp	From front wall
6	0 mm	200 mm
1	240 mm	440 mm
2	480 mm	680 mm
3	720 mm	920 mm
4	960 mm	1160 mm
5	1200 mm	1400 mm

As shown in Figure 9, for Tencate GX60/30 the typical locations of the six points of measurements is shown in Table 3.

Table 3. Typical locations of the six-point measurements for Tencate GX60/30

LVDT No.	From clamp	From front wall
6	0 mm	200 mm
1	100 mm	300 mm
2	200 mm	400 mm
3	300 mm	500 mm
4	400 mm	600 mm
5	500 mm	700 mm

The five LVDTs were connected to specific locations on the geogrid tested. Concerning Tensar RE580, the spacing between measuring points was 240 mm and 125 mm for Tencate Miragrid GX60/30. The thin 2 mm rods attached to the transverse ribs were connected to the LVDTs. These cables passed through the holes at the back wall with rubber O-rings to ensure that the water remains sealed inside the soil chamber especially for undrained loading condition. The remaining space in the soil chamber was filled with soil leaving a 100 mm gap for the air bag. The soil was compacted at every 150 mm lift and tested using the electronic soil density gauge. Thereafter, the topmost level of the compacted soil was covered with rubber inflatable airbag that was connected to an air pump with a pressure gage assembly. The soil chamber was then covered with a reinforced steel plate. To simulate the overburden pressure, the inflatable airbag was pressurized to the desired pressure level and held constantly until the entire pullout test was terminated regardless of the loading condition. Once the desired air bag pressure was achieved, the pullout force was applied to the soil-geogrid setup for the drained loading condition at a constant displacement rate of 1 mm/min.

3. Results and Discussion

The main materials were evaluated and tested individually to determine its properties and baseline data that were then used in the pullout test. The laboratory test results of CGS and FGS are shown in Table 4.

Table 4. Laboratory test properties of CGS and FGS

CGS	FGS
USCS : SP (poorly graded sand)	USCS: CL – sandy clays with low to medium plasticity
Gravel: 6.82%	Gravel: 1.86%
Sand: 90.66%	Sand: 24.98%
Fines: 2.53%	Fines: 73.16%
Max. dry density: 2081 kg/m^3	LL: 41.84%
Optimum moisture: 8.75%	PL: 20.36%
Cu: .01	Max dry density: 1506.6kg /m^3
Cc: 0.92	Optimum moisture: 21.91%

The strength envelopes of the described soils of CGS and FGS are shown in Figures 10 and 11, respectively.

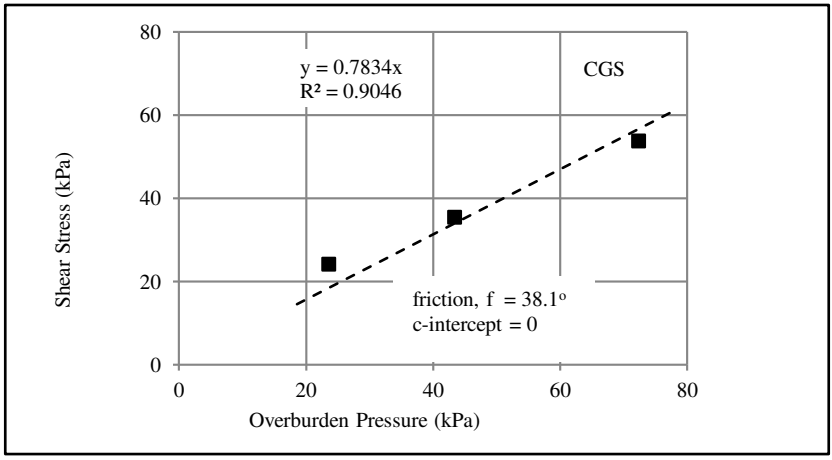

Figure 10. Shear strength envelope of CGS

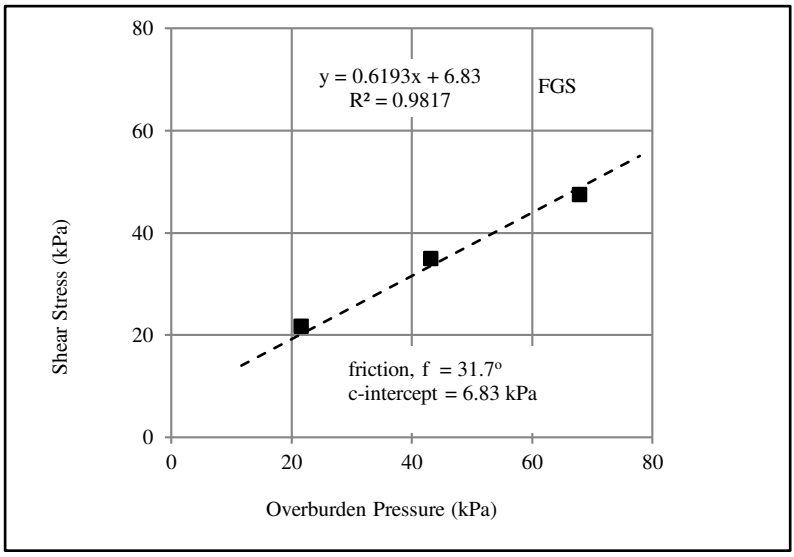

Figure 11. Shear strength envelope of FGS

The two geogrid reinforcements used in this research were tested independently using the wide width tensile test in order to establish their respective stress-strain relationships to be used later in the pullout test.

Tensar RE580 shown in Figure 12 had high density polyethylene (HDPE) with a unit weight of 0.98 kg/m^2 and long term strength (ULS or Tcr) of 59.17 kN/m. Stress-strain relationship is shown in Figure 13.

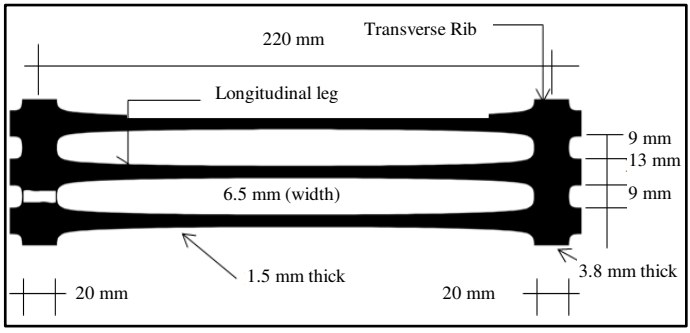

Figure 12. Dimension of a typical portion of Tensar RE580

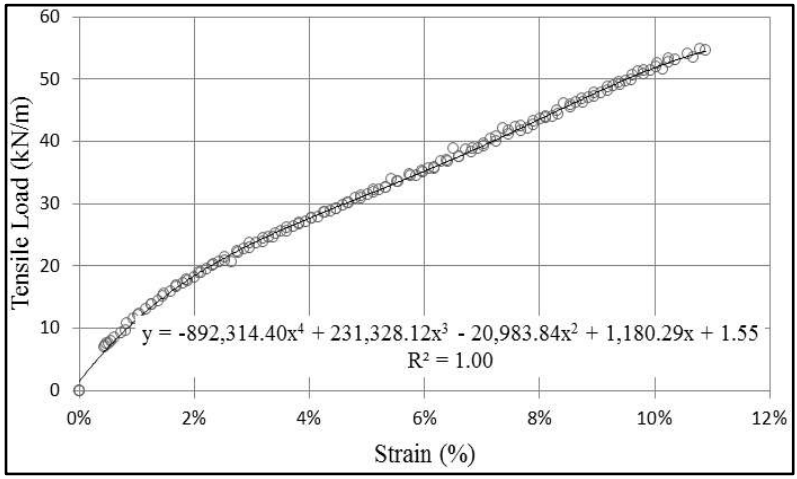

Figure 13. Stress-strain relationship of Tensar RE580

Tencate Miragrid GX60/30 shown in Figure 14 was made of polymer-coated polyester yarn (PPY) with ultimate strength (Tu) at 10% strain of 60kN/m, strength at 5% strain of 30 kN/m and unit weight of 0.25kN/m^2. Stress-strain relationship is shown in Figure 15.

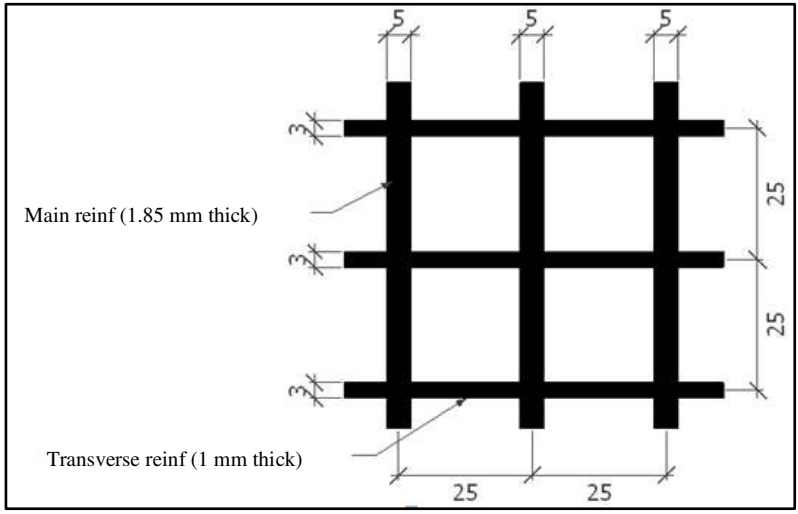

Figure 14. Dimension of a typical portion of Tencate GX60/30

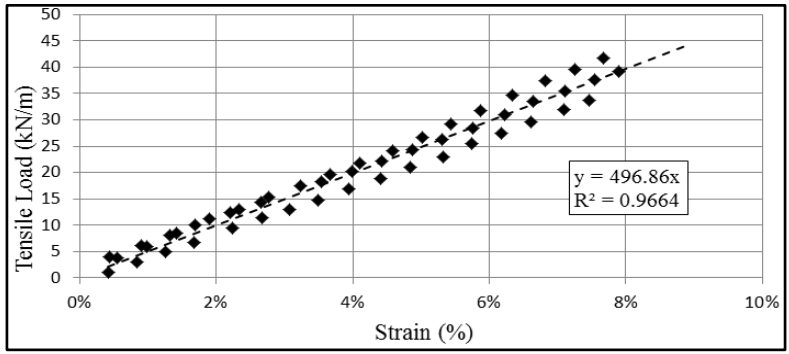

Figure 15. Stress-strain relationship of Tencate GX60/30

After establishing the individual material properties of the soils and geogrid reinforcements, a series of pullout tests were conducted for drained and undrained loading conditions for the different types of geogrids and soils, and effective overburden pressures as summarized in Table 1. The load-displacement graphs are shown in Figures 16 to 19 for the pullout tests conducted for undrained and drained loading conditions with measurement taken in front of the Tensar RE580 geogrid specimen. The same process was carried out for the Tencate GX60/30 geogrid, but is not shown in this paper. Every load-displacement curve was a function of the pullout force, overburden pressure (OBP), and pore pressure (PP) for undrained loading.

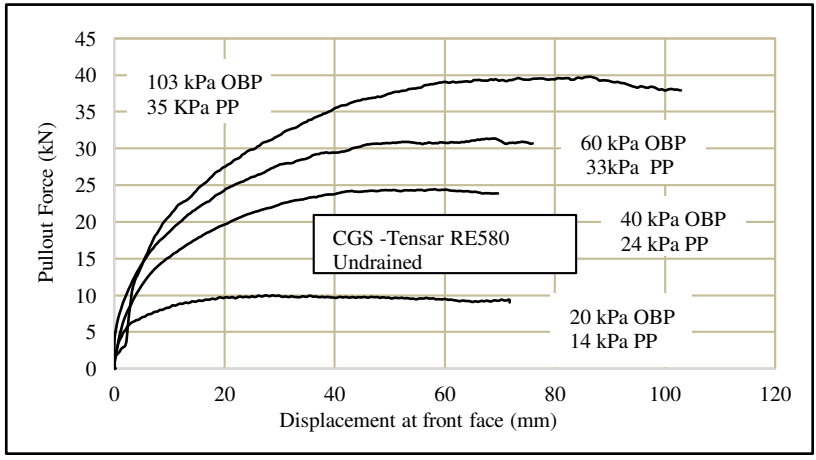

Figure 16. Load-displacement curve for CGS-Tensar RE580 under undrained loading

Whether the loading condition was drained or undrained, the characteristics of the load-displacement curves were the same. The load was proportional to the overburden pressure. As the overburden pressure increased, the pullout force also increased. The pullout capacities were reached at higher displacements for higher overburden pressures for both types of geogrids for all types of soil samples and both drainage conditions. At the same time, the pullout force for the undrained loading was lower compared with the drained loading for the same overburden pressure.

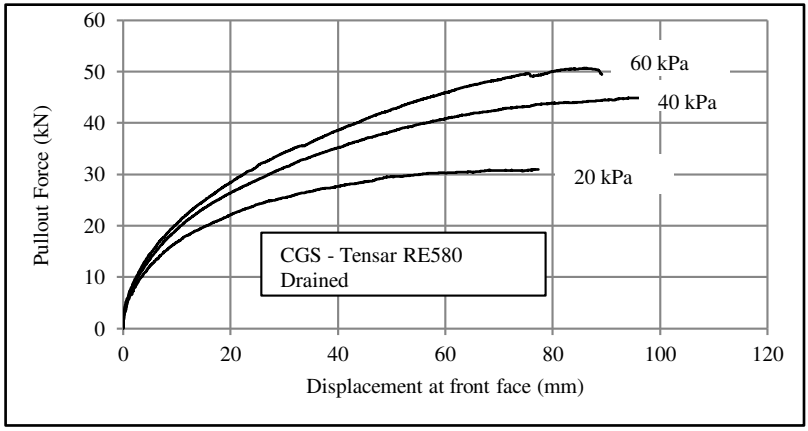

Figure 17. Load-displacement curve for CGS-Tensar RE580 under drained loading

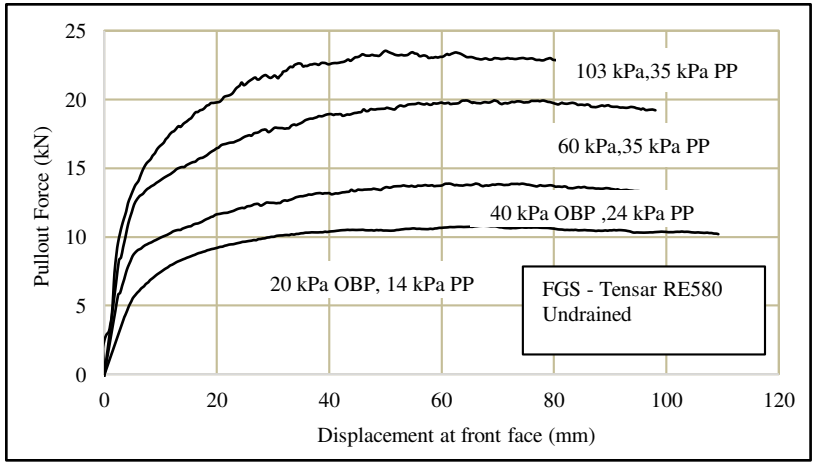

Figure 18. Load-displacement curve for FGS-Tensar RE580 under undrained loading

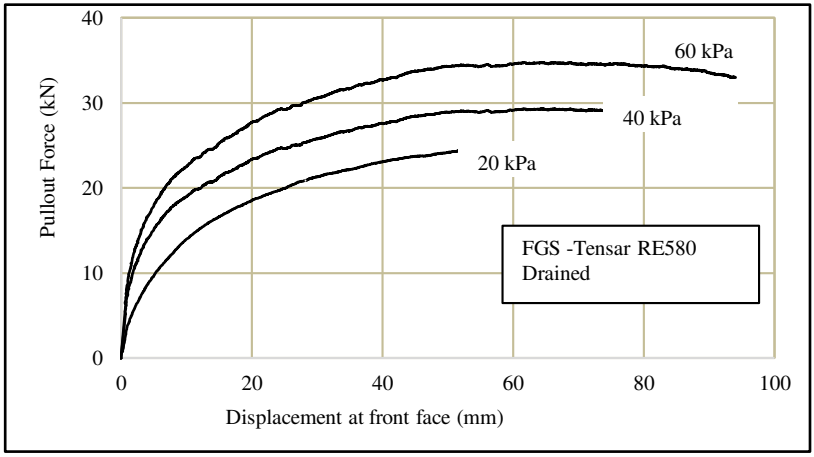

Figure 19. Load-displacement curve for FGS-Tensar RE580 under drained loading

The load-displacement curves for the different test setup were used to determine the soil-geogrid strength envelopes in terms of apparent cohesion intercept (c_{ap}) and apparent friction angle (d_{ap}) as shown in Figures 20 and 21 for CGS-Tensar RE580 undrained and drained loading. Table 5 shows the summary of the apparent interaction parameters of the different soil-geogrid setup for both drained and undrained conditions.

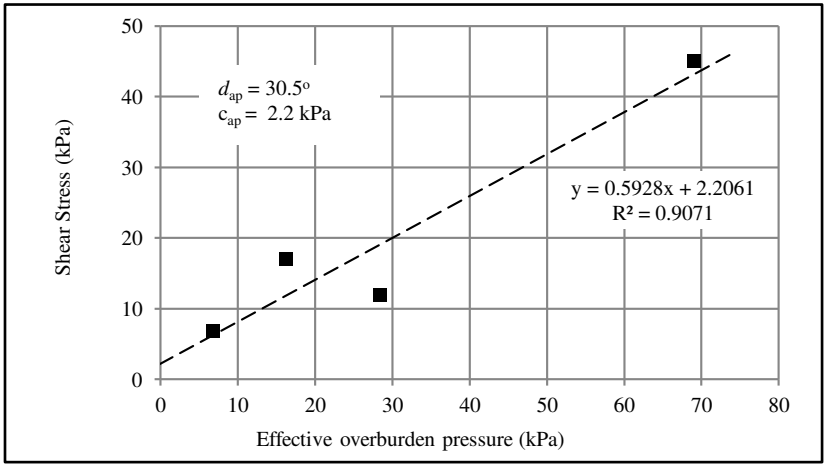

Figure 20. Pullout strength envelope for CGS-Tensar RE580 under undrained loading

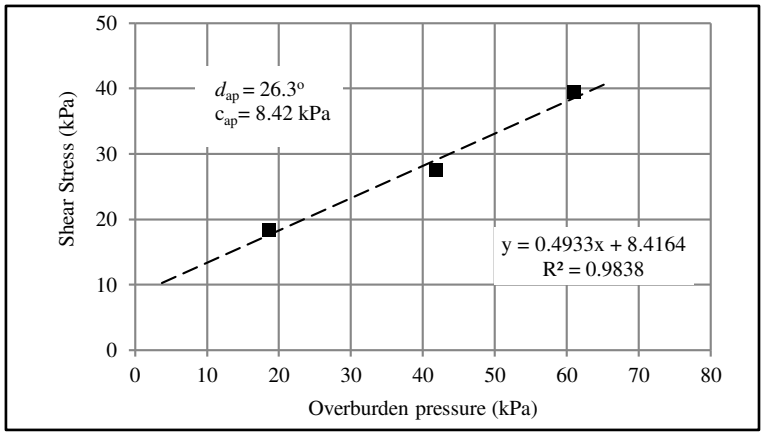

Figure 21. Pullout strength envelope for CGS-Tensar RE580 under drained loading

Table 5. Summary apparent interaction parameters for different test setup

Soil	Geogrid	Setup	Cohesion Intercept (C_{ap})	Interface Friction Angle (d_{ap})
CGS	Tensar RE580	Drained	8.40	26.30
CGS	Tensar RE580	Undrained	2.00	30.50
FGS	Tensar RE580	Drained	13.13	11.70
FGS	Tensar RE580	Undrained	7.50	15.80
CGS	Tencate GX60/30	Drained	21.90	28.60
CGS	Tencate GX60/30	Undrained	18.40	27.40
FGS	Tencate GX60/30	Drained	12.00	21.50
FGS	Tencate GX60/33	Undrained	8.80	20.90

Figure 22 shows the summary of the pullout strength envelopes for Tensar RE580 interfaced with CGS and FGS for drained and undrained loading condition. The graph for Tencate Miragrid GX60/30 interfaced with CGS and FGS for drained and undrained loading is shown in Figure 23. The graphs show the relationships between apparent strength envelopes the drained and undrained conditions.

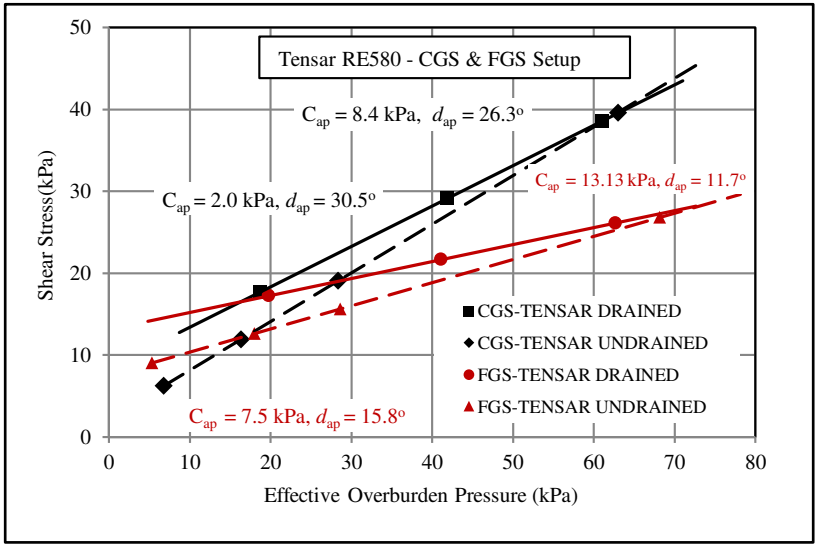

Figure 22. Summary plots of calculated pullout strength envelopes for Tensar RE580 interfaced with CGS and FGS

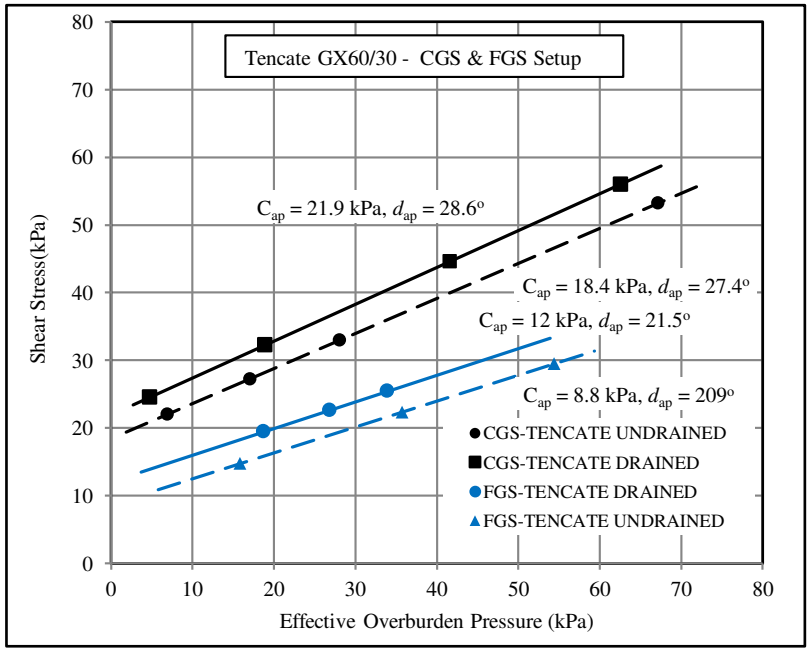

Figure 23. Summary plots of calculated pullout strength envelopes for Tencate GX60/30 interfaced with CGS and FGS

For the Tensar setup interfaced with CGS and FGS, the behavior and interaction of the geogrid were very similar but of different values as shown in Figure 22. It was observed that there was a higher strength envelope values for CGS-Tensar setup than the FGS-Tensar setup. This was expected since the friction angles of CGS were always higher than that of the FGS, even if the CGS cohesion values were lower than the FGS values.

At higher overburden pressures greater than 60 kPa, the undrained strength envelope values started to exceed the drained strength envelope values in both CGS and FGS setup. The undrained condition as observed had slightly higher friction angle than the drained condition.

There was a notable difference in the interaction of Tencate with CGS and FGS as shown in Figure 23. The CGS-Tencate setup has higher strength envelopes than the FGS-Tencate setup for both drained and undrained condition. Furthermore, the friction angles for CGS-Tencate setup had slightly higher friction angles than that for FGS-Tencate setup, while their cohesion values differed significantly. Since the strength envelopes were relatively parallel for each type of setup, the differences between the drained and undrained condition were basically the net cohesion for each CGS-Tencate and FGS-Tencate setup.

3.1 Coefficient of Interaction

By definition, the coefficient of interaction (Ci) is the ratio of the apparent pullout resistance to the shear strength of the soil backfill taken from the laboratory's direct shear test. Most of the design methods for reinforced soil structures are based on limit equilibrium method and the interaction properties are evaluated using the average resistance method. In this study, the apparent pullout resistance was evaluated by the average resistance (T_{av}) method using the total area method shown in Equation 1.

$$Ci = \frac{T_{av}}{T_{ss}} \tag{1}$$

where:

T_{av} = average pullout resistance
T_{ss} = direct shear resistance of soil-to-soil

For the different effective overburden pressures, the actual shear strengths (T_{av}) were calculated using Equation 2, and consequently determined the coefficients of interaction for the two types of geogrids and interfaced with the CGS and FGS for both drained and undrained loading conditions as shown in Table 6.

$$T_{av} = \frac{F_{Tmax}}{2 \cdot B \cdot L} \tag{2}$$

where:

F_{Tmax} = pullout resistance
B = width of geogrid
L = length of geogrid

Table 6. Summary of calculated interaction coefficients

Setup	Drainage Condition	Apparent cohesion (kPa)	Apparent Friction Angle (degree)	Effective Overburden pressure (kPa)	Actual Shear Strength (kPa)	Interaction Coefficient (Ci)
CGS - Tensar RE580	Non-Submerged (Drained)	8.40	26.30	18.73	18.35	1.19
				41.84	27.51	0.87
				61.02	39.35	0.79
	Submerged (Undrained)	2.20	30.70	6.75	6.76	1.16
				16.33	16.90	0.92
				28.39	11.78	0.84
				63.00	44.89	0.79
FGS - Tensar RE580	Non-Submerged (Drained)	13.13	11.70	19.81	16.74	0.83
				41.11	22.68	0.64
				62.68	25.65	0.55
	Submerged (Undrained)	7.50	15.80	5.30	9.56	0.76
				17.98	13.35	0.64
				28.61	13.93	0.60
				68.18	27.40	0.53
CGS-Tencate GX60/30	Non-Submerged (Drained)	21.90	28.60	4.73	19.50	6.52
				18.90	37.70	2.15
				41.60	47.02	1.35
				62.52	53.16	1.13
	Submerged (Undrained)	18.40	27.40	6.87	20.68	4.02
				17.03	25.47	2.01
				28.07	37.15	1.48
				67.16	51.98	1.00
FGS-CGS-Tencate GX60/30	Non-Submerged (Drained)	12.02	21.52	18.72	19.51	0.96
				26.82	22.38	0.90
				33.89	25.50	0.86
	Submerged (Undrained)	8.66	20.95	15.81	13.56	0.80
				35.70	24.71	0.73
				54.34	28.23	0.70

It can be noticed that the corresponding Ci for undrained condition were always lower than the Ci of the drained condition for the same given effective overburden pressures. Generally, the Ci for both drainage conditions decreased as the overburden pressure increased for all test setup. As expected, the CGS-soil setup possessed higher Ci values compared with FGS-soil setup for any type of geogrid. It can also be noted that Ci values above 1.0, especially for the CGS-Tencate GX60/30, showed that its shear strengths were higher and more efficient than the soil-to-soil shear strength. Figures 24 and 25 show the graphs for both setups.

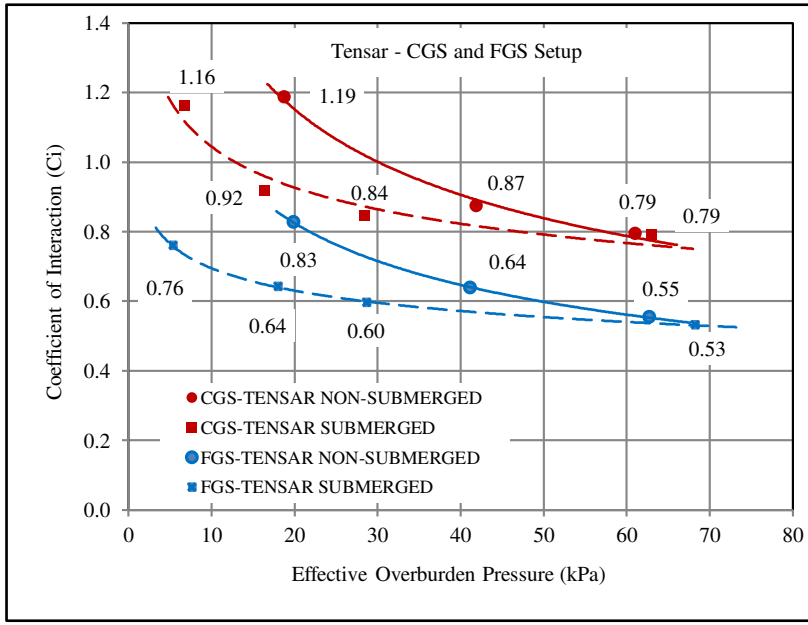

Figure 24. Coefficient of interaction curves for FGS and CGS interfaced with Tensar RE580

Noticeably, the test results revealed a significant reduction of the Ci from non-submerged to submerged conditions for the same soil-geogrid test setup. The reduced values were more pronounced at lower effective overburden pressures (EOBP) (e.g. at EOBP < 40 kPa). On the other hand, the Ci values for both drained and undrained conditions gradually became equal at higher effective overburden pressures starting at 60 kPa.

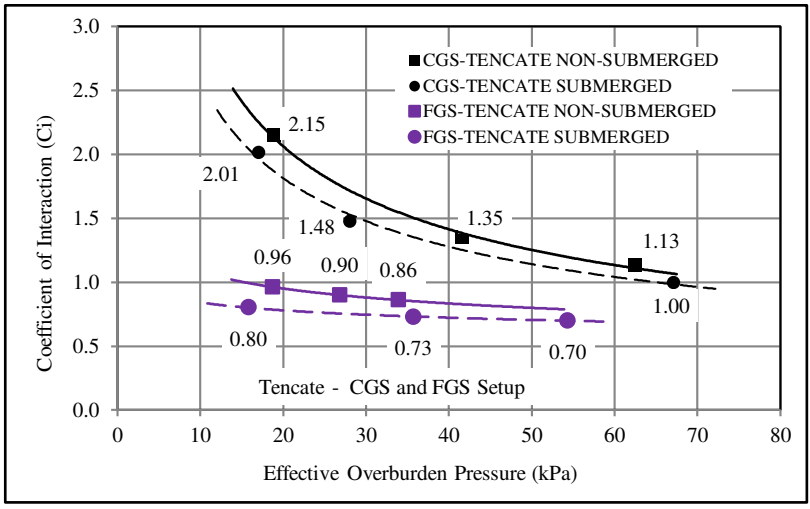

Figure 25. Coefficient of interaction curves for FGS and CGS interfaced with Tencate GX60/30

This means that the coefficient of interaction did not remain constant when the soil-geogrid was submerged even at the same amount of effective overburden pressures. The reduction of Ci values for submerged conditions was significant at low effective overburden pressures for Tensar RE580 at 37% for CGS and 43% for FGS compared with Tencate GX60/30 at 14% for CGS and 22% for FGS. Therefore, this reduction was critical to the design of MSE walls that may be submerged in its design life.

By regression analysis, the equations of the interaction coefficients (Ci) were established for different effective overburden pressures for the design of the MSE walls for both and non-submerged (C_{iD}) and submerged (C_{iUD}) conditions. Equations 3, 4, 5, and 6 were used for CGS-Tensar RE580, FGS-Tensar RE580, CGS-Tencate GX60/30 and FGS-Tencate GX60/30, respectively.

$$Ci_D = 3.2426 \cdot (\sigma'_n)^{-0.35}$$
$$C_{UD} = 1.5518 \cdot (\sigma'_n)^{-0.17} \quad (3)$$

$$Ci_D = 2.3502 \cdot (\sigma'_n)^{-0.35}$$
$$C_{UD} = 0.9592 \cdot (\sigma'_n)^{-0.14} \quad (4)$$

$$Ci_D = 10.539 \cdot (\sigma'_n)^{-0.55} \quad (5)$$
$$C_{UD} = 8.2362 \cdot (\sigma'_n)^{-0.51}$$

$$Ci_D = 1.6717 \cdot (\sigma'_n)^{-0.188} \quad (6)$$
$$C_{UD} = 1.0838 \cdot (\sigma'_n)^{-0.11}$$

4. Conclusion and Recommendation

In conclusion, there was a significant reduction of the design parameters in the submerged conditions, especially at lower effective overburden pressures as compared with the submerged conditions for the same effective overburden pressures. The implication of this is to use lower interaction coefficients (Ci) for MSE structures that are expected to be submerged instead of uniformly using the Ci values recommended for non-submerged conditions for different values of overburden pressures as it is usually the practice in designing for MSE walls.

Although the design of MSE structures that are partially or fully submerged applies the principle of effective stress while using the coefficient of interaction based on drained conditions, as supplied by the manufacturer for general types of soil, is generally acceptable, the effect of the submergence is not considered in the design practice and thus overestimates the coefficient of interaction used especially at fairly low overburden pressures. Based on the foregoing premises, complemented with the above conclusions, the following are the recommendations:

4.1 Application of Submerged Pullout Test Method and Results for Effective Design of MSE Structures

The equations presented in the conclusion for submerged conditions would be a good starting point and consequently, can be used for the design and evaluation of MSE structures for marine application, specifically for the geogrids used in this study. The recommended interaction coefficients include a good comparison for submerged and non-submerged conditions.

The test method in this study for submerged condition can be adopted to establish a database table of Ci values with equations for other commercially available geogrids in the market, which at the moment is not yet available, except for the geogrids used in this work.

The pullout test for submerged condition in this study can also be applied to geotextiles, steel grids, and metallic strips as soil reinforcements to MSE structures.

Indigenous geogrids of organic origin such as coconets can be evaluated using the submerged pullout test procedure since the application of the material for low height MSE structures is highly suitable.

Since the pullout test results for submerged FGS is already available, reusing FGS that are more available on site, instead of importing CGS, can be confidently applied. This is very attractive for the potential cost savings for the project.

4.2 Other Application of Submerged Pullout Test Procedure

The study can be extended further to a variation of pore pressure for every overburden pressure for each soil-geogrid setup and chosen type of soil, specifically for the fine-grained soils. This will help the engineers in evaluating MSE structures that may experience constant fluctuation of saturation, such as after a heavy downpour from the mountain slopes or tidal changes on quay walls. It is also recommended to determine the distribution of friction and passive bearing forces while considering the effects of submerged conditions for soil reinforcements with or without transverse ribs.

Improvements can be introduced to the pullout testing machine to identify other beneficial information. Pressure transducers can be added at the location of the soil-geogrid interface to determine the actual overburden pressure at that level. Lastly, vertical displacement transducers may also be installed to determine possible consolidation of the soil, especially for fine grained soils.

5. Acknowledgement

This work would have not been completed without the people who made significant contributions. The main author have had a wonderful time with his adviser and very dear friend, Dr. Glen A. Lorenzo, who gave his support and direction. Dr. Jonathan C. Maglasang provided guidance in designing the electro-mechanical system of the large-scale pullout testing equipment. Dr. Dennes T. Bergado shared input to the scope and extent of the research that gave authors deeper understanding on the workings and behavior of geosynthetics as soil reinforcements for MSE structures. Finally, the main

author owes an incalculable debt to his loving wife, Sheila, and wonderful children, Katherine and Isaiah John, for their unyielding support.

6. References

Alfaro, M.C., Hayashi, S., Miura, N., & Watanabe, K. (1995a). Pullout interaction mechanism of geogrid strip reinforcement. Geosynthetics International, 2(4), 679-698. https://doi.org/10.1680/gein.2.0030

Alfaro, M.C., Miura, N., & Bergado, D.T., (1995b), Soil geogrid reinforcement interaction by pullout and direct shear tests. Geotechnical Testing Journal, 18(2), 157-167. https://doi.org/10.1520/GTJ10319J

American Society for Testing and Materials (ASTM) C127-01. (2001). Test method for permeability of granular soils (constant head). West Conshohocken, PA: ASTM International.

American Society for Testing and Materials (ASTM) C128-01. (2001). Test method for determining the specific gravity of fine aggregate. ASTM. West Conshohocken, PA: ASTM International.

American Society for Testing and Materials (ASTM) D1556-00. (2000). Standard test method density and unit weight of soil in place by sand cone method. West Conshohocken, PA: ASTM International.

American Society for Testing and Materials (ASTM) D4318-10. (2010). Standard test methods for liquid limit, plastic limit, and plasticity index of soils. West Conshohocken, PA: ASTM International.

American Society for Testing and Materials (ASTM) D2487-11. (2011). Classification of soils for engineering purposes. West Conshohocken, PA: ASTM International.

American Society for Testing and Materials (ASTM) D3080-04. (2004). Standard test method for direct shear test of soils under consolidated drained condition. ASTM. Philadelphia, PA, USA.

American Society for Testing and Materials (ASTM) D422-63. (1998). Standard test method for particle-size analysis of soils. ASTM. West Conshohocken, PA: ASTM International.

American Society for Testing and Materials (ASTM) D6706-01. (2001). Standard test method for measuring geosynthetic pullout resistance in soil. West Conshohocken, PA: ASTM International.

American Society for Testing and Materials (ASTM) D698-00a. (2003). Standard test method for laboratory compaction characteristics of soils using standard effort (12,400 ft-lbf/ft^3 (600 kN-m/m^3). West Conshohocken, PA: ASTM International.

Bathurst, R.J., Allen, T.M., & Walters, D.L. (2005). Reinforcement loads in geosynthetic walls and the case for new working stress design method. Geotextiles and Geomembranes, 5 (3), 287-322. https://doi.org/10.1016/j.geotexmem.2005.01.002

Berg, R.R., Christopher, B.R., & Samtani, N.C. (2009). Design and construction of mechanically stabilized earth walls and reinforced soil slopes (Vol. 1). Washington, DC: US Department of Transportation Federal Highway Administration.

Bergado, D.T., Bukkanasuta, A., & Balasubramaniam, A.S. (1986). Laboratory pull-out test using bamboo and geogrid polymer including a case study. Geotextiles and Geomembranes, 5(3), 153-189. https://doi.org/10.1016/0266-1144(87)90015-X

Bergado, D.T., Chai, J.C., Abiera, H.O., Alfaro, M.C., & Balasubramaniam, A.S. (1993). Interaction between cohesive-frictional soil and various grid reinforcements. Geotextiles and Geomembranes, 12(4), 327-349. https://doi.org/10.1016/0266-1144(93)90008-C

Bergado, D.T., Chai, J.C., & Miura, N. (1996). Prediction of pullout resistance and pullout force-displacement relationship of inextensible grid reinforcements. Soil and Foundations, 36(4), 11-22. https://doi.org/10.3208/sandf.36.4_11

Bergado, D.T., Lo, K.H., Chai, J.C., Shivashankar, R., Alfaro, M.C., & Anderson, L.R. (1992). Pullout tests using steel grid reinforcements with low quality backfill. Journal of Geotechnical Engineering, 118(7), 679-698. https://doi.org/10.1061/(ASCE)0733-9410(1992)118:7(1047)

Bergado, D.T., Sampaco, C.L., Alfaro, M.C., & Balasubramaniam, A. (1988). Welded-wire reinforced earth (mechanically stabilized embankments) with cohesive backfill on soft clay. Bangkok, Thailand: USAID.

Bobet, A. (2002). Design of MSE walls for fully saturated conditions. Retrieved from https://docs.lib.purdue.edu/cgi/viewcontent.cgi?article=1522&context=jtrp

Bowles, J.E. (1997). Foundation analysis and design. New York: McGraw-Hill.

Duszynska, A., & Bolt, A. (2004). Pullout tests of geogrid embedded in non-cohesive soil. Archives of Hydro-Engineering and Environmental Mechanics, 51(2), 135-147.

Esfandiari, J., & Selamat, M.R. (2012). Laboratory investigation on the effect of transverse member on pullout capacity of metal strip reinforcement in sand. Geotextiles and Geomembranes, 35, 41-49. https://doi.org/10.1016/j.geotexmem.2012.07.002

Farrag, K., & Morvant, M.J. (2004). Evaluation of interaction properties of geosynthetics in cohesive soils: Lab and field Tests. Retrieved from https://rosap.ntl.bts.gov/view/dot/22384/dot_22384_DS1.pdf?

Hossain, M.Z., & Sakai, T. (2007). A study on pullout behavior of reinforcement due to variation of water content of soil. Agricultural Engineering International: CIGR Ejournal, 9, 1-15.

Jewell, R.A. (1996). Soil reinforcement with geotextiles. London: Construction Industry Research and Information Association.

Jewell, R.A., Palmeira, E.M., Milligan, G.W.E., Sarsby, R.W., & Dubois, D. (1984). Interaction between soils and geogrids. Proceedings of the Symposium on Polymer Grid Reinforcement in Civil Engineering, Institution of Civil Engineering, London, 18-30.

Koerner, R.M. (2005). Designing with geosynthetics. Upper Saddle River, NJ, New Jersey: Pearson Prentice Hall.

Lajevardi, S.H., Dias, D., & Racinais, J. (2013). Analysis of soil-welded steel mesh reinforcement by pull-out tests. Geotextiles and Geomembranes, 40, 48-57. https://doi.org/10.1016/j.geotexmem.2013.08.002

Lopes, M.J., & Lopes, M.L. (1999). Soil-geosynthetic interaction – Influence of soil particle size and geosynthetic structure. Geosynthetics International, 6(4), 261-282. https://doi.org/10.1680/gein.6.0153

Matsui, T., San, K.C. Nabeshima, Y., & Amin, U.N. (1996). Bearing mechanism of steel grid reinforcement in pullout test. Proceedings of the International Symposium on Earth Reinforcement Fukuoka, Kyushu, Japan, 101-105.

Minažek, K., & Mulabdić, M. (2013). A review of soil reinforcement interaction testing in reinforced pullout test. Gradevinar, 65, 235-250.

Mitchell, J.K., & Zornberg, J.G., (1995). Reinforced soil structures with poorly draining backfills Part II: Case histories and applications. Geosynthetics International, 2(1), 265-307. https://doi.org/10.1680/gein.2.0011

Montanelli, F., & Recalcati, P. (2003). The design of reinforced soil retaining walls using TENAX geogrids. Vigano, Italy: TENAX.

Moraci, N., & Cardile, G. (2009). Influence of cyclic tensile loading in pullout resistance of geogrids embedded in a compacted granular soils. Geotextiles and Geomembranes, 27(6), 475-487. https://doi.org/10.1016/j.geotexmem.2009.09.019

Moraci, N., & Cardile, G. (2012). Deformative behaviour of different geogrid embedded in a granular soil under monotonic and cyclic pullout loads. Geotextiles and Geomembranes, 32(3), 104-110. https://doi.org/10.1016/j.geotexmem.2011.11.001

Moraci, N., Cardile, G., Gioffre, D., Mandaglio, M.C., Calvarano, L.S., & Carbone, L. (2014). Soil geosynthetic interaction: Design parameters from experimental and theoretical analysis. Transportation Infrastructure Geotechnique, 1, 165-227. https://doi.org/10.1007/s40515-014-0007-2

Moraci, N., & Gioffre, D. (2006). A simple method to evaluate the pullout resistance of extruded geogrids embedded in compacted granular soil. Geotextiles and Geomembranes, 24(2), 116-128. https://doi.org/10.1016/j.geotexmem.2005.11.001

Moraci, N., & Recalcati, P. (2006). Factors affecting the pullout behaviour of extruded geogrids embedded in compacted granular soils. Geotextiles and Geomembranes, 24(4), 220-242. https://doi.org/10.1016/j.geotexmem.2006.03.001

Muller-Rochholz, J., & Recker, C., (2000). Tensile strength and clamping of geogrids. In P.E. Stevenson (Ed.), Grips, clamps, clamping techniques, and strain measurement for testing of geosynthetics (pp. 28-36). West Conshohocken, PA: American Society for Testing and Materials.

Nayeri, A., & Fakharian, K. (2009). Study on pullout behaviour of uniaxial HDPE geogrids under monotonic and cyclic loads. International Journal of Civil Engineering, 7(4), 211-223.

Ochiai, H., Otani, J., Hayahiw, S., & Hirai, T. (1996). The pull-out resistance of geogrids in reinforced soil. Geotextiles and Geomembranes, 14(1), 19-42. https://doi.org/10.1016/0266-1144(96)00027-1

Palmeira, E.M., & Milligan, G.W.E. (1989). Scale and other factors affecting the results of pullout tests of grid buried in sand. Geotechnique, 39(3), 511-524. https://doi.org/10.1680/geot.1989.39.3.511

Palmeira, E.M. (2007). Soil-geosynthetic interaction: Modelling and analysis. Retrieved from https://www.mercerlecture.com/-/media/Files/Mercer/Pdf/Palmeira-Edinburgh.ashx?la=en

Peterson, L.M., & Anderson, L.R. (1980). Pullout resistance of welded wire mesh embedded in soil. Logan, Utah: Utah State University.

Rimoldi, P., Ricutti, A., & Ricalcati, P. (1994). TENAX geosynthetics technical literature, design manual: Steep reinforced slopes. Vigano, Italy: TENAX.

Sieira, A.C.C.F, Gerscovich, D.M.S., & Sayao, A.S.F.J. (2009). Displacement and load transfer mechanisms of geogrids under pullout condition. Geotextiles and Geomembranes, 27(4), 241-251.

U.S. Department of Transportation and Federal Highway Administration. (2001). Mechanically stabilized earth walls and reinforced soil slopes design and construction guidelines. Washington, DC: National Highway Institute Office of Bridge Technology.

Zhou, J., Chen, J.F., Xue, J.F., & Wang, J.Q. (2012). Micro-mechanism of the interaction between sand and geogrid transverse ribs. Geosynthetics International, 19(6), 426-437. https://doi.org/10.1680/gein.12.00028